Journal of Applied Physics ARTICLE scitation.org/journal/jap

Energy storage in $BaBi_4Ti_4O_{15}$ thin films with high efficiency

Cite as: J. Appl. Phys. **125**, 134101 (2019); doi: 10.1063/1.5086515
Submitted: 21 December 2018 · Accepted: 19 March 2019 ·
Published Online: 1 April 2019

D. P. Song,[1,a)] J. Yang,[2] B. B. Yang,[3] Y. Wang,[1] L.-Y. Chen,[1] F. Wang,[1] and X. B. Zhu[3,b)]

AFFILIATIONS

[1]Department of Physics, Jiangsu University of Science and Technology, Zhenjiang 212003, People's Republic of China
[2]School of Materials Science and Engineering, Jiangsu University of Science and Technology, Zhenjiang 212003, People's Republic of China
[3]Key Laboratory of Materials Physics, Institute of Solid State Physics, Chinese Academy of Sciences, Hefei 230031, People's Republic of China

[a)]**Electronic mail:** dpsong@just.edu.cn
[b)]**Electronic mail:** xbzhu@issp.ac.cn

ABSTRACT

A ferroelectric film with slim polarization-electric (P-E) hysteresis loops, showing small remanent polarization (P_r) and large saturated polarization (P_s), is desired to obtain high recoverable energy density (U_{re}) and efficiency (η) in thin film capacitors. Here, small P_r and large P_m values are achieved in $BaBi_4Ti_4O_{15}$ thin films through modulating film grain size. A large U_{re} of 44.3 J/cm^3 as well as a high η of 87.1% is obtained. In addition, the derived $BaBi_4Ti_4O_{15}$ thin films show excellent energy storage performance in wide frequency range, thermal stability, and fatigue endurance. These results suggest that $BaBi_4Ti_4O_{15}$ films can be considered as a candidate for dielectric energy storage capacitors, and the route through grain size optimization is a promising strategy to improve the capacitive performance of ferroelectric materials.

I. INTRODUCTION

Dielectric capacitors, featured by an extremely short discharge time (on a microsecond scale), are special electrical energy storage devices and enable many pulsed power applications, such as medical defibrillators, hybrid electric vehicles, and advanced electromagnetic systems.[1] Recently, ferroelectric thin film capacitors have attracted intensive research interest due to their high electrical energy densities, wide temperature stability, and outstanding fatigue endurance.[2] Generally, a typical ferroelectric, which shows rectangular polarization (P)-electric field (E) hysteresis loops with large remanent polarization (P_r) that approaches saturated polarization (P_s), can be used for electric energy storage applications.

According to $U_{re} = \int_{P_r}^{P_s} EdP$, a high recoverable energy density U_{re} and efficiency η can be simultaneously achieved in a ferroelectric film with a small P_r and a large P_s, which usually has a slim polarization-electric (P-E) hysteresis loop.[3] Several approaches have been reported to slim down the P-E loops of ferroelectric thin films, including interface- or domain-engineering,[4,5] space-charges or solid solution,[6,7] a seed or dead layer,[8,9] multilayer and nanocomposites,[10,11] compositions near phase boundaries or alloying,[12,13] anti- and relaxor ferroelectrics.[14–16] Through optimization, U_{re} and η have been improved rapidly to 20–70 J/cm^3 and 60%–80% (even higher), respectively. The recoverable energy density in thin films is about one order higher than the bulk counterparts. In addition, crystalline quality or grain size has a very important effect on remanent polarization of thin films. A transition of ferroelectric hysteresis loops from square loops to slim loops is observed with decreasing grain size.[17] With decreasing the grain size, a smaller value of P_r is obtained due to the reduced contributions of both the extrinsic domain wall and the intrinsic lattice.[18] Annealing time and annealing temperature are considered as the most effective methods to control the crystallization quality and crystallite size. Recently, a phase-field model combined with a finite element method suggests that both the discharge energy density and the energy storage efficiency of ferroelectric ceramics can be enhanced with a decrease in the grain size at their breakdown points.[19]

Here, the Aurivillius ferroelectric $BaBi_4Ti_4O_{15}$ thin films with various grain sizes have been deposited on Pt/Si substrates by annealing at different temperatures with the same dwell time.[20] The ferroelectric hysteresis loops of these films change obviously with the variations in the grain size, benefitting for the significant reduction of P_r. As a result, a large U_{re} of 44.3 J/cm^3 and a high η of 87.1%, together with a low dielectric loss and a high dielectric constant, are obtained in $BaBi_4Ti_4O_{15}$ thin films. Additionally, the optimized thin film shows good thermal stabilities and fatigue endurance. It is indicated that the optimization of the grain size could be an effective strategy to improve the capacitive performance of ferroelectrics.

II. EXPERIMENTAL PROCEDURE

$BaBi_4Ti_4O_{15}$ (BBT) thin films were fabricated on Pt/Si substrates by the chemical solution deposition (CSD) method, as schemed in Fig. 1(a). The precursor solution was composed of metal acetates, tetrabutyl titanate, and propionic acid and then heated and stirred vigorously. The ratio of raw materials according to stoichiometry except 5% bismuth excess is used to compensate for volatility during processing. Before spin coating, the substrates were cleaned ultrasonically in acetone, alcohol, and de-ionized water in sequence. The spin speed is 6000 rpm and the spin time is 20 s. After spin coating, the wet films were baked for 10 min at 400 °C in a preheated tube furnace. The film thickness was increased with repeated spin coating and baking processing. The baked films were annealed for 30 min in ambient atmosphere at 550−700 °C with an interval of 50 °C. For the sake of simplicity, the thin films annealed at 550 °C are denoted as BBT55 and so on. The crystal structure of thin films was examined by X-ray diffraction (XRD, Shimadzu) analysis with monochromatic Cu-K_α radiation at room temperature. The microstructure and cross-sectional morphologies were observed using a field-emission scanning electron microscope (FE-SEM, Sirion 200 type, FEI Company, USA). Dielectric, leakage, and ferroelectric properties were examined with a precision

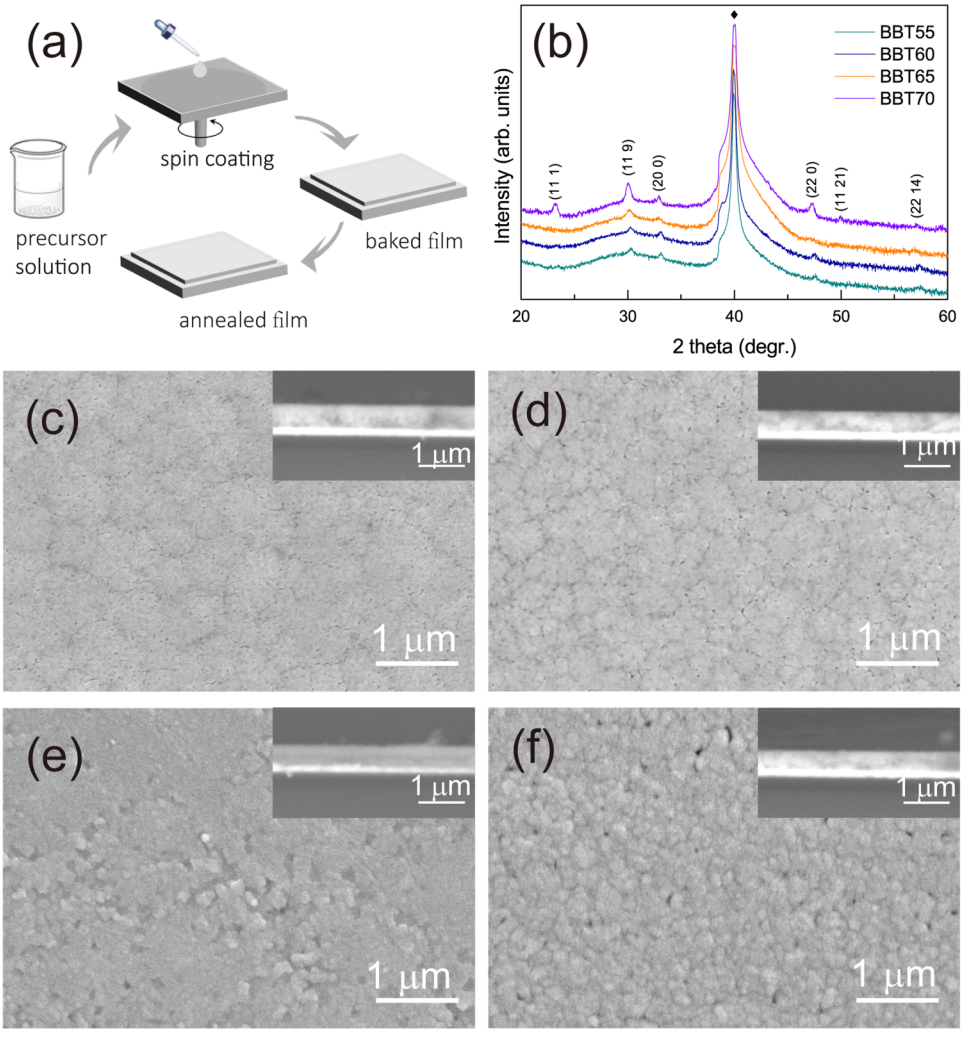

FIG. 1. (a) Film deposition schematic, (b) XRD patterns, and (c)–(f) FE-SEM images for BBT thin films annealing at different temperatures. Details are (c) BBT55, (d) BBT60, (e) BBT65, (f) BBT70, and the insets show the corresponding cross-sectional morphologies to determine the film thickness. The black diamond represents the diffraction peak of the substrate.

impedance analyzer (TH2828/A/S, Tonghui Electronic, China) with a perturbation voltage of 500 mV and a computer-controlled standardized ferroelectric test system attached to a Sawyer-Tower circuit (Precision Premier II, Radiant Technology, USA).

III. RESULT AND DISCUSSION

Figure 1(b) shows the XRD patterns of BBT thin films deposited on platinum coated silicon substrates with different annealing temperatures. The results show that all the films are of single-phase polycrystalline and can be indexed with an orthorhombic lattice with the space group $A2_1am$, which is consistent with the previous results.[16] With the increasing annealing temperature, enhanced diffraction intensity and sharper peaks suggest improved crystallinity as well as increased crystalline size. To demonstrate the annealing temperature effects on the crystallite size and the microstructure of all thin films, FE-SEM measurements are carried out, and their corresponding results are shown in Figs. 1(c)–1(f). It can be seen that the surface morphology of all the films is considerably smooth and dense. Along with the increase of the annealing temperature, the grain size shows a remarkable enhancement, and the grain boundaries become clearer. When the annealing temperature is lower than 650 °C, the surface morphology exhibits blurred grain boundaries implying a very small grain size and much intergrain connectivity of the adjacent grains. The average grain sizes of the films are evaluated to be sub-10 nm, 17, 28, and 45 nm according to the FE-SEM pictures. It needs to be stated that the grain boundaries of the lower temperature annealing films are extremely ambiguous due to their incomplete crystallization, thus the values given above are approximated. The film thickness is determined as ∼ 450 nm, and it is gradually decreased with the increasing annealing temperature, which may be attributed to the enhancement in the thermal energy effects.

It is consensus that a high permittivity is necessary for high energy storage density. Figure 2(a) represents the results of frequency dependent dielectric constant ε_r and loss $\tan\delta$, which are

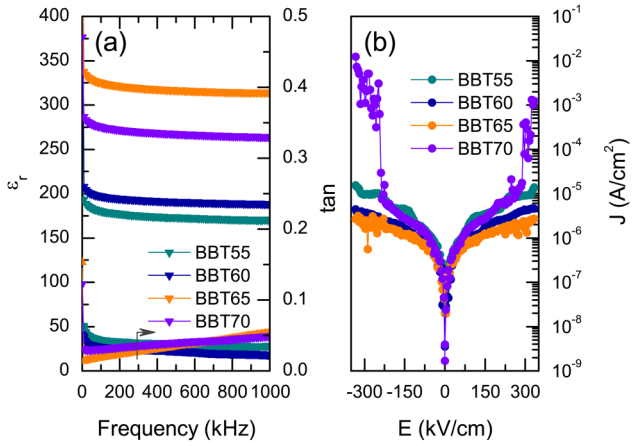

FIG. 2. (a) Frequency dependence of dielectric constant ε_r and loss $\tan\delta$, (b) leakage current J-E curves in semilog scales for all the derived thin films at room temperature.

measured in the frequency range of 0.01–1 MHz and a driving voltage of 500 mV at RT. As the frequency increases, ε_r is gradually decreased. The declined tendency of ε_r for all samples was caused by the insufficient mobility of dipoles, leading to the contribution of the dipoles, such as space charge, which can be suppressed at higher frequencies.[21,22] ε_r gradually increases before 650 °C and then decreases with the further increase of the annealing temperature to 700 °C. The results of the enhanced ε_r with the increasing annealing temperature can be attributed to the enhancement in the grain size and a consequent decrease in grain boundaries.[23,24] Nevertheless, the defects (usually oxygen vacancies) will increase with increasing annealing temperature, which will result in a decrease in ε_r. As shown in Fig. 2(b) of the leakage current density J in a semilog scale, it is seen that J is decreased with the annealing temperature when the annealing temperature is below 650 °C due to the improvements in the crystal quality as well as thin film density. Furthermore, J is increased with a further increase of the annealing temperature due to the increased defects. In addition, the development of crystalline grain with increasing annealing temperature will reduce the grain boundary, which will increase J since the grain boundary is more insulating than the film itself in most cases.[25,26] Thus, the competition of the two effects, i.e., grain size and defects, will lead to the variation of the ε_r in BBT thin films with annealing temperature. On the other hand, the $\tan\delta$ values of all the derived thin films are very small, which are below 0.05. In low frequencies ($<$ 500 kHz), combined with leakage data, the lowest $\tan\delta$ of BBT65 indicates that the main contribution is of conduction.[27] Under high frequencies ($>$ 800 kHz), the tendency of $\tan\delta$ is first increased and then decreased with the increasing annealing temperature, which is similar with ε_r. This suggests that the $\tan\delta$ in the high frequency mainly depends on the motion and reversal of domain walls.[28] For the BBT65 thin films, it has a large ε_r of 314 and a low $\tan\delta$ of 0.05 due to a small J of 2.7×10^{-6} A/cm^2, which is similar to the previous works.[29]

The room-temperature polarization-electric field (P-E) hysteresis loops of BBT thin films measured under the applied electric field up to 2 MV/cm and the applied frequency of 10 kHz are shown in Figs. 3(a)–3(d). The P-E hysteresis loops of BBT thin films transform from slanted ones to a nearly saturated loop with the annealing temperature increasing from 550 to 700 °C. The maximum polarization P_m (defined as the polarization at the maximum electric field here) is increased monotonously with the increasing annealing temperature, while the remanent polarization P_r (defined as the polarization at zero electric fields) initially decreases until 650 °C, and then increases substantially at the annealing temperature of 700 °C. For the displacement type ferroelectrics under enough field amplitude, the spontaneous P_m is dominated by the lattice structure and crystallization quality.[30,31] As a result, P_m increases with increasing annealing temperature due to the improved crystalline quality. However, P_r is much more complicated: the initial decrease of P_r is owing to the effect of small grain size and decline leakage current density, and the substantial increase in BBT70 is attributed to the growth of the crystalline grain.[18,32] A nearly saturated P-E loop with the remanent polarization P_r of 11 μC/cm^2 under 2 MV/cm in BBT70 thin films is an advantage to previous reports, suggesting the reliable quality of the derived BBT thin films.[20] For the low temperature annealed BBT thin films, it is observed from

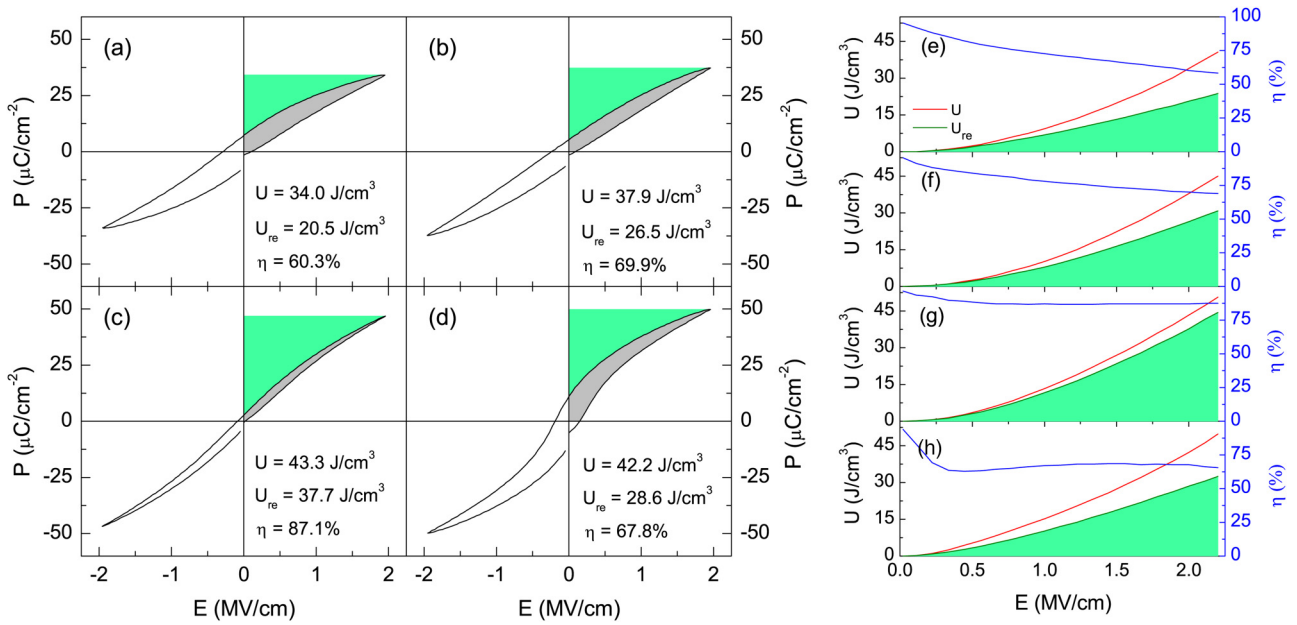

FIG. 3. Room-temperature P-E hysteresis loops with a measured frequency of 10 kHz for (a) BBT55, (b) BBT60, (c) BBT65, and (d) BBT70. Electric field amplitude dependence of energy density and the corresponding energy efficiency η of the (e) BBT55, (f) BBT60, (g) BBT65, and (h) BBT70. The recoverable energy density (U_{re}) and loss energy density (U_{loss}) are represented by the green and gray area, respectively.

Figs. 3(a) to 3(c) that the P-E loops become more and more slender with the increase in P_m and decreases P_r, which are beneficial for energy storage applications.

The energy storage density (U) of ferroelectric materials can be expressed as $U = U_{re} + U_{loss}$ and the energy efficiency is $\eta = U_{re}/U$.[1] The U_{loss} represents the amount of energy density dissipated during the discharge process, illustrated by the gray shaded area in Fig. 3. The U_{re} can be calculated by integrating the effective area between the discharging curve of the P-E loops and the polarization axis, shown by the green shaded area in Fig. 3. As shown in Figs. 3(a)–3(d), U, U_{re}, and η are all included in the calculation of the homologous P-E loop results. The BBT65 thin film performs excellently in the energy storage property with $U_{re} = 37.7\,\mathrm{J/cm^3}$ and $\eta = 87.1\%$ under 2 MV/cm. The U_{re} reaches a comparable level with much lead-based and lead-free ferroelectric thin film capacitors, but the η reported here is also higher.[6–9,13,14,16,22,28,33–38] It seems that the BBT70 thin film shows $U = 42.2\,\mathrm{J/cm^3}$, which is comparable to BBT65 $U = 43.3\,\mathrm{J/cm^3}$, yet the η of former is just 67.8%. For a more clear and comprehensive comparison, the electric field dependent U, U_{re}, and η are tracked and displayed on the right side of Fig. 3 for all BBT thin films. It can be seen that both U and U_{re} are monotonously increased with increasing applied electric field, especially in the high field area. The η of the lower temperature annealed samples shows a gradual decrease with increasing applied electric field in Figs. 3(e) and 3(f). The higher annealing samples displayed in Figs. 3(g) and 3(h) give a stable platform after the initial stage of decline with increasing applied electric field. The electric field stability of η implies that such BBT thin films can be used as lead-free ferroelectric thin film capacitors in energy storage applications.[2] Particularly, the film of BBT65 exhibits better multiple parameter features such as larger energy storage density (a maximum green area) and higher efficiency (a high flat horizontal line) under the same electric field amplitude.

Figure 4 shows the relative measured results of frequency, fatigue, temperature, and breakdown electric field of BBT65 thin film as a candidate of dielectric energy storage capacitors. The frequency dependence of P-E hysteresis loops is carried out at the field amplitude of 1.3 MV/cm and RT. The excellent frequency dependent ferroelectric properties are obviously obtained as shown in Figs. 4(a) and 4(d).[33,38] The P_m and P_r decrease from 34.9 to $32.8\,\mu\mathrm{C/cm^2}$ and from 2.8 to $2.7\,\mu\mathrm{C/cm^2}$ with the increasing measurement frequency, respectively. Figure 4(b) gives the P-E hysteresis loops before and after 1.3×10^8 charge/discharge cycles under a field amplitude of 1.3 MV/cm and a frequency of 10 kHz at RT. The corresponding P_m and P_r are displayed in Fig. 4(d), and there are negligible changes of P_r but a decrease from 33.5 to $31.8\,\mu\mathrm{C/cm^2}$ of P_m, resulting in the slight decrease of U_{re} and η to $16.8\,\mathrm{J/cm^3}$ and 80.8% compared to those before the fatigue test of $17.8\,\mathrm{J/cm^3}$ and 82.4%, respectively. Such results indicate good fatigue endurance of BBT65 thin films, which is an important parameter expected for ferroelectric capacitors in energy storage applications.[14,28]

Another important factor for applications is the thermal stability of ferroelectric thin film capacitors, and good thermal stability can not only broaden the application scope of devices but also reduce the overall cost by removing the cooling accessories.[7,39]

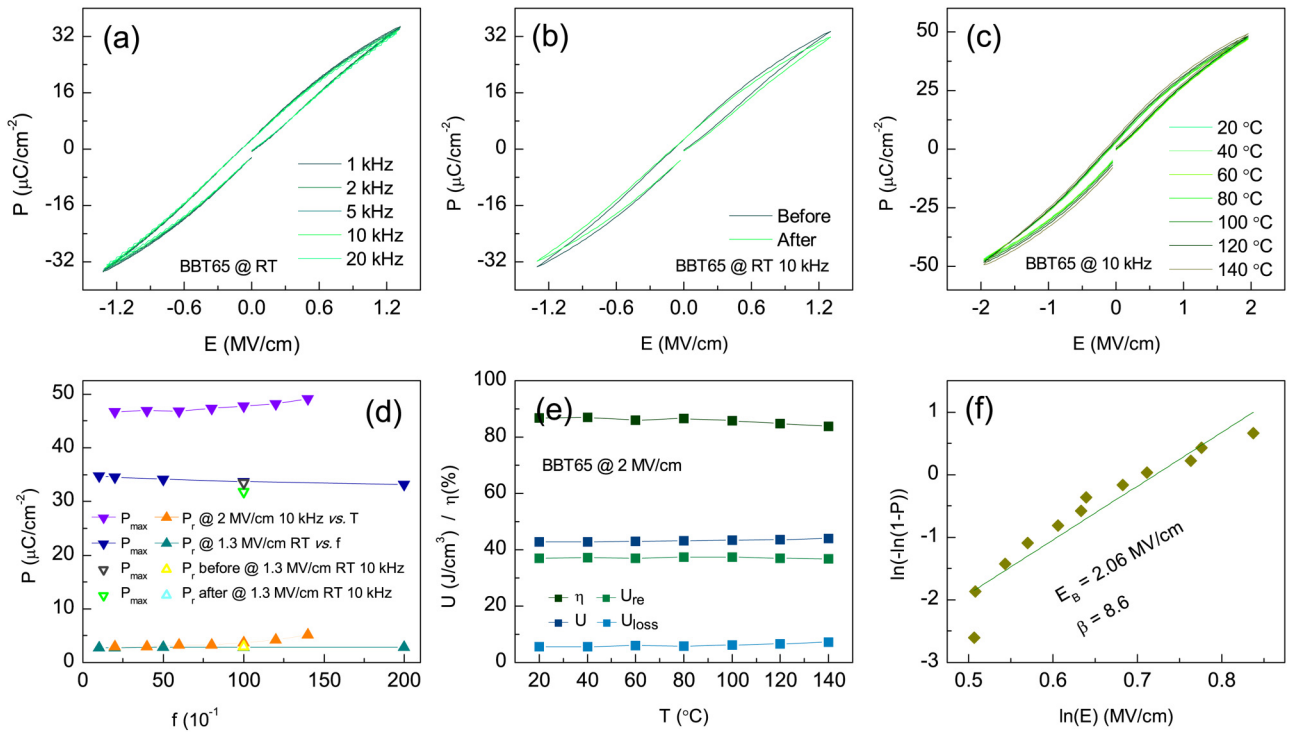

FIG. 4. The P-E hysteresis loops of BBT65 thin films at (a) different frequencies, (b) before and after 1.3×10^8 charge/discharge cycles, and (c) temperature from 20 to 140 °C. (d) The variation of U_{re} and η corresponding to those P-E hysteresis loops. (e) The energy storage performance of U, U_{re}, U_{loss}, and η depending on the temperature. (e) Weibull distributions and the fitting results of breakdown electric field.

The thermal stability of the BBT65 thin film is checked by collecting its P-E hysteresis loops at a temperature from 20 to 140 °C. The obtained P-E loops as shown in Fig. 4(c) reveal a very insignificant broadening tendency with increasing temperature, demonstrating its outstanding thermal stability. A slight upward trend of P_m and P_r on the temperature shown in Fig. 4(d) can be attributed to the fact that ferroelectric domains are easy to move and reversal due to higher thermal energy at elevated temperatures.[33,40] The temperature dependent energy storage performance is calculated from the P-E loops and shown in Fig. 4(e). The reduction of U_{re} and η are only 0.5% and 3%, which is slightly decreased 37.1 J/cm^3 and 86.7% to 36.9 J/cm^3 and 83.8% under the electric field of 2.0 MV/cm. These results signify that the deterioration of energy storage performance is almost negligible. For the comparison in energy storage performances with other lead-free thin film systems, the η of BBT65 thin films around 87% (at 20 °C) and 84% (at 140 °C) is much higher with moderate recoverable energy density.[7,14,16,22,28,34–38] Finally, for dielectric energy storage capacitors, the statistical breakdown strength is also examined by statistical investigation of the Weibull distribution as shown in Fig. 4(f).[7,41] The calculated breakdown electric field is approximately 2.06 MV/cm here. The obtained breakdown strengths are comparable to those reported previously for the lead-free films. The Weibull modulus β associated with the linear regressive fit of the distribution is 8.6, representing less scattering in the experimental data indicating few defects in the film.[42]

IV. CONCLUSIONS

In summary, four-layered Aurivillius family $BaBi_4Ti_4O_{15}$ thin films were deposited on Pt/Si substrates by the CSD route. The ferroelectric and energy storage properties of the BBT thin films were investigated. The well-saturated ferroelectric hysteresis loops with $2P_r$ more than 20 μC/cm^2 were obtained in BBT70 thin films. The slim polarization-electric hysteresis loop with large P_m and small P_r in BBT65 thin films resulting in a large U_{re} of 44.3 J/cm^3 and a high η of 87.1% is favorable to capacitor's energy storage applications. The polarization in the broadband frequency, thermal stability at evaporation temperature, and fatigue endurance after charge/discharge cycles are also addressed. These results suggest that BBT thin films can be considered as lead-free ferroelectric capacitors in energy storage applications.

ACKNOWLEDGMENTS

This work was supported by the National Natural Science Foundation of China (NNSFC) (Grant Nos. 11847093 and 51801077), the Jiangsu Province Science Foundation for Youths (No. BK20160561), the Jiangsu Educational Committee (Grant No.

17KJB140006), and the Scientific Research Foundation of JUST (Grant Nos. 1052931611 and 1052921801).

REFERENCES

[1]Z. Yao, Z. Song, H. Hao, Z. Yu, M. Cao, S. Zhang, M. T. Lanagan, and H. Liu, Adv. Mater. **29**, 1601727 (2017).
[2]H. Palneedi, M. Peddigari, G.-T. Hwang, D.-Y. Jeong, and J. Ryu, Adv. Funct. Mater. **28**, 1803665 (2018).
[3]B. J. Chu, X. Zhou, K. Ren, B. Neese, M. Lin, Q. Wang, F. Bauer, and Q. M. Zhang, Science **313**, 334 (2006).
[4]Z. Sun, C. Ma, M. Liu, J. Cui, L. Lu, J. Lu, X. Lou, L. Jin, H. Wang, and C.-L. Jia, Adv. Mater. **29**, 1604427 (2017).
[5]H. Cheng, J. Ouyang, Y.-X. Zhang, D. Ascienzo, Y. Li, Y.-Y. Zhao, and Y. Ren, Nat. Commun. **8**, 1999 (2017).
[6]W. Zhang, Y. Q. Gao, L. M. Kang, M. L. Yuan, Q. Yang, H. B. Cheng, W. Pan, and J. Ouyang, Acta Mater. **85**, 207 (2015).
[7]H. Pan, Y. Zeng, Y. Shen, Y.-H. Lin, J. Ma, L. Li, and C.-W. Nan, J. Mater. Chem. A **5**, 5920–5926 (2017).
[8]Z. K. Xie, Z. X. Yue, B. Peng, J. Zhang, C. Zhao, X. H. Zhang, G. Ruehl, and L. T. Li, Appl. Phys. Lett. **106**, 202901 (2015).
[9]M. McMillen, A. M. Douglas, T. M. Correia, P. M. Weaver, M. G. Cain, and J. M. Gregg, Appl. Phys. Lett. **101**, 242909 (2012).
[10]J. Li, F. Li, Z. Xu, and S. Zhang, Adv. Mater. **30**, e1802155 (2018).
[11]Y. Zeng, Z.-H. Shen, Y. Shen, Y. Lin, and C.-W. Nan, Appl. Phys. Lett. **112**, 103902 (2018).
[12]B. Peng, Q. Zhang, X. Li, T. Sun, H. Fan, S. Ke, M. Ye, Y. Wang, W. Lu, H. Niu, J. F. Scott, X. Zeng, and H. Huang, Adv. Electron. Mater. **1**, 1500052 (2015).
[13]S. Cho, C. Yun, Y. S. Kim, H. Wang, J. Jian, W. Zhang, J. Huang, X. Wang, H. Wang, and J. L. MacManus-Driscoll, Nano Energy **101**, 398 (2018).
[14]M. H. Park, H. J. Kim, Y. J. Kim, T. Moon, K. D. Kim, and C. S. Hwang, Adv. Energy Mater. **4**, 1400610 (2014).
[15]B. Xu, J. Iniguez, and L. Bellaiche, Nat. Commun. **8**, 15682 (2017).
[16]J. Y. Chen, Z. H. Tang, B. Yang, and S. F. Zhao, Appl. Phys. Lett. **113**, 153904 (2018).
[17]H. Amorin, R. Jimenez, J. Ricote, T. Hungria, A. Castro, and M. Alguero, J. Phys. D Appl. Phys. **43**, 285401 (2010).
[18]L. Jin, F. Li, S. Zhang, and D. J. Green, J. Am. Ceram. Soc. **97**, 1 (2014).
[19]Z. Cai, X. Wang, W. Hong, B. Luo, Q. Zhao, and L. Li, J. Am. Ceram. Soc. **101**, 5487–5496 (2018).
[20]K. M. Satyalakshmi, M. Alexe, A. Pignolet, N. D. Zakharov, C. Harnagea, S. Senz, and D. Hesse, Appl. Phys. Lett. **74**, 603 (1999).
[21]D. William, D. Callister, and G. Rethwisch, *Materials Science and Engineering: An Introduction* (John Wiley & Sons, New York, 2009), p. 992.
[22]B. B. Yang, M. Y. Guo, D. P. Song, X. W. Tang, R. H. Wei, L. Hu, J. Yang, W. H. Song, J. M. Dai, X. J. Lou, X. B. Zhu, and Y. P. Sun, Appl. Phys. Lett. **111**, 183903 (2017).
[23]D. P. Song, X. W. Tang, B. Yuan, X. Z. Zuo, J. Yang, L. Chen, W. H. Song, X. B. Zhu, and Y. P. Sun, J. Am. Ceram. Soc. **97**, 3857 (2014).
[24]Z. Song, H. X. Liu, S. J. Zhang, Z. J. Wang, Y. T. Shi, H. Hao, M. H. Cao, Z. H. Yao, and Z. Y. Yu, J. Eur. Ceram. Soc. **34**, 1209 (2014).
[25]H. Chen, B. Shen, J. Xu, and J. Zhai, J. Alloy Compd. **551**, 92 (2013).
[26]F. Rehman, J.-B. Li, M.-S. Cao, Y.-J. Zhao, M. Rizwan, and H.-B. Jin, Ceram. Int. **41**, 14652 (2015).
[27]D. B. Sirdeshmukh, L. Sirdeshmukh, and K. G. Subhadra, *Micro- and Macro-Properties of Solids: Thermal, Mechanical and Dielectric Properties* (Springer, New York, 2006), p. 202.
[28]J. Y. Chen, Z. H. Tang, Y. L. Bai, and S. F. Zhao, J. Alloy Compd. **675**, 257 (2016).
[29]R. Z. Hou, X. M. Chen, and Y. W. Zeng, J. Am. Ceram. Soc. **89**, 2839 (2006).
[30]S. C. Abrahams, S. K. Kurtz, and P. B. Jamieson, Phys. Rev. **172**, 551 (1968).
[31]Q. Yu, J.-F. Li, Y. Chen, L.-Q. Cheng, W. Sun, Z. Zhou, Z. Wang, and G. Brennecka, J. Am. Ceram. Soc. **97**, 107 (2014).
[32]R. Jiménez, H. Amorín, J. Ricote, J. Carreaud, J. Kiat, B. Dkhil, J. Holc, M. Kosec, and M. Algueró, Phys. Rev. B **78**, 094103 (2008).
[33]G. Hu, C. Ma, W. Wei, Z. Sun, L. Lu, S. Mi, M. Liu, B. Ma, J. Wu, and C. Jia, Appl. Phys. Lett. **109**, 193904 (2016).
[34]Y. Zhang, W. Li, Y. Qiao, Y. Zhao, Z. Wang, Y. Yu, H. Xia, Z. Li, and W. Fei, Appl. Phys. Lett. **112**, 093902 (2018).
[35]P. Chen, S. Wu, P. Li, J. Zhai, and B. Shen, J. Eur. Ceram. Soc. **38**, 4640 (2018).
[36]Z. Lin, Y. Chen, Z. Liu, G. Wang, D. Rmiens, and X. Dong, J. Eur. Ceram. Soc. **38**, 3177 (2018).
[37]Z. Sun, C. Ma, X. Wang, M. Liu, L. Lu, M. Wu, X. Lou, H. Wang, and C. L. Jia, ACS Appl. Mater. Interfaces **9**, 17096 (2017).
[38]N. Sun, Y. Li, Q. Zhang, and X. Hao, J. Mater. Chem. C **6**, 10693 (2018).
[39]F. Yan, H. Yang, L. Ying, and T. Wang, J. Mater. Chem. C **6**, 7905 (2018).
[40]R. C. Miller and G. Weinreich, Phys. Rev. **117**, 1460 (1960).
[41]Z. Liang, M. Liu, C. Ma, L. Shen, L. Lu, and C.-L. Jia, J. Mater. Chem. A **6**, 12291 (2018).
[42]X. Zhang, Y. Shen, B. Xu, Q. Zhang, L. Gu, J. Jiang, J. Ma, Y. Lin, and C. W. Nan, Adv. Mater. **28**, 2055 (2016).